Temporal and Vertical Oxygen Gradients Modulate Nitrous Oxide Production in a Seasonally Anoxic Fjord: Saanich Inlet, British Columbia

Ji, Q., Jameson, B.D., Juniper, S.K., & Grundle, D.S.

2020

JGR Biogeosciences

RESEARCH ARTICLE
10.1029/2020JG005631

Temporal and Vertical Oxygen Gradients Modulate Nitrous Oxide Production in a Seasonally Anoxic Fjord: Saanich Inlet, British Columbia

Qixing Ji[1,2,3], Brett D. Jameson[4], S. Kim Juniper[4,5,6], and Damian S. Grundle[3]

[1]School of Marine Sciences, Sun Yat-Sen University, Zhuhai, China, [2]GEOMAR, Helmholtz Centre for Ocean Research Kiel, Kiel, Germany, [3]Bermuda Institute of Ocean Sciences, St. George's, Bermuda, [4]School of Earth and Ocean Sciences, Bob Wright Centre, University of Victoria, Victoria, British Columbia, Canada, [5]Department of Biology, University of Victoria, Victoria, British Columbia, Canada, [6]Ocean Networks Canada, Victoria, British Columbia, Canada

Abstract Nitrous oxide (N_2O) is a strong greenhouse gas and an ozone depleting agent. In marine environments, N_2O is produced biologically via ammonium oxidation, nitrite, and nitrate reduction. The relative importance of these principle production pathways is strongly influenced by oxygen availability. We conducted ^{15}N tracer experiments of N_2O production in parallel with measurements of N_2O concentration and natural abundance isotopes/isotopomers in Saanich Inlet, a seasonally anoxic fjord, to investigate how temporal and vertical oxygen gradients regulate N_2O production pathways and rates. In April, June, and August 2018, the depth of the oxic-anoxic interface (dissolved oxygen = 2.5 μmol L^{-1} isoline) progressively deepened from 110 to 160 m. Within the oxygenated and suboxic water column, N_2O supersaturation coincided with peak ammonium oxidation activity. Conditions in the anoxic deep water were potentially favorable to N_2O production from nitrate and nitrite reduction, but N_2O undersaturation was observed indicating that N_2O consumption exceeded rates of production. In October, tidal mixing introduced oxygenated water from outside the inlet, displacing the suboxic and anoxic deep water. This oxygenation event stimulated N_2O production from ammonium oxidation and increased water column N_2O supersaturation while inhibiting nitrate and nitrite reduction to N_2O. Results from ^{15}N tracer incubation experiments and natural abundance isotopomer measurements both implicated ammonium oxidation as the dominant N_2O production pathway in Saanich Inlet, fueled by high ammonium fluxes (0.6–3.5 nmol m^{-2} s^{-1}) from the anoxic depths. Partial denitrification contributed little to water column N_2O production because of low availability of nitrate and nitrite.

Key Points:
- Ammonium oxidation is the dominant N_2O production pathway in suboxic Saanich Inlet
- Addition of nitrate and nitrite stimulates N_2O production in anoxic, N_2O-depleted deep water
- Oxygenation of anoxic water enhances N_2O production via ammonium oxidation and increases water column N_2O supersaturation level

Supporting Information:
- Supporting Information S1

Correspondence to:
Q. Ji,
jiqixing@mail.sysu.edu.cn

Citation:
Ji, Q., Jameson, B. D., Juniper, S. K., & Grundle, D. S. (2020). Temporal and vertical oxygen gradients modulate nitrous oxide production in a seasonally anoxic fjord: Saanich Inlet, British Columbia. *Journal of Geophysical Research: Biogeosciences*, *125*, e2020JG005631. https://doi.org/10.1029/2020JG005631

Received 5 JAN 2020
Accepted 25 JUL 2020
Accepted article online 28 AUG 2020

Author Contributions:
Conceptualization: Qixing Ji, Damian S. Grundle
Formal analysis: Qixing Ji
Funding acquisition: Damian S. Grundle
Investigation: Qixing Ji, Brett D. Jameson, Damian S. Grundle
Methodology: Qixing Ji, S. Kim Juniper, Damian S. Grundle
Supervision: Damian S. Grundle
Visualization: Qixing Ji
Writing - original draft: Qixing Ji, Brett D. Jameson, S. Kim Juniper, Damian S. Grundle
Writing – review & editing: Qixing Ji, Brett D. Jameson, S. Kim Juniper, Damian S. Grundle

1. Introduction

Nitrous oxide (N_2O) is an important atmospheric trace gas that regulates Earth's climate through catalysis of stratospheric ozone depletion (Crutzen, 1970) and absorption of long wave radiation (Yung et al., 1976). Globally, N_2O is mostly produced by biological activities (Codispoti, 2010), such that understanding the N_2O cycling pathways and associated regulating factors is a prerequisite for N_2O budget estimates, particularly in the marine environment (Bange et al., 2019; Wilson et al., 2018). The biological production of N_2O is attributed to nitrogen cycling processes, during which N_2O can be produced as a by-product of aerobic oxidation of ammonium (NH_4^+) to nitrite (i.e., the first step of nitrification) and as an important intermediate during the anaerobic reduction of nitrate (NO_3^-) and nitrite (NO_2^-). Consumption of N_2O occurs under anoxic conditions where heterotrophic bacteria reduce N_2O to N_2. Over 40% of natural N_2O emissions occur in marine and freshwater environments (Ciais et al., 2013). Notably, high N_2O emissions are often associated with steep vertical oxygen gradients (oxyclines), such as those found in open ocean oxygen minimum zones (OMZs) with nanomolar oxygen at intermediate depths, and eutrophic coastal waters (Bange et al., 1996; Buitenhuis et al., 2018). While open ocean N_2O emission estimates are relatively well constrained (Buitenhuis et al., 2018), coastal emissions are highly uncertain (Maavara et al., 2019), primarily due to highly variable spatial and temporal gradients of dissolved oxygen concentration (DO) and organic matter export (de Bie et al., 2002; Laperriere et al., 2019). Projecting future N_2O emission scenarios requires a better understanding of the spatial and temporal dynamics of N_2O production in relation to environmental variability, especially in productive coastal environments.

Saanich Inlet, a well-studied seasonally anoxic fjord, was chosen as the experimental site to investigate how temporal and vertical variability of dissolved oxygen regulates N_2O production in coastal waters. Located on southern Vancouver Island in British Columbia, Canada, Saanich Inlet has a central deep basin (~215 m) and a shallow sill (~70 m) at its north facing mouth, which restricts deepwater movement in and out of the fjord (Herlinveaux, 1962). Spring-neap tidal mixing at the seaward end of the fjord introduces new nutrients (primarily NO_3^-) to the surface waters of Saanich Inlet on a fortnightly basis (Gargett et al., 2003), resulting in high new primary production (Grundle & Juniper, 2011; Grundle et al., 2009). Rapid sinking of particulate organic matter and subsequent remineralization cause water column deoxygenation (Timothy & Soon, 2001), creating a steep oxycline on top of the anoxic bottom water where hydrogen sulfide (H_2S) accumulates (Cohen, 1978; Torres-Beltrán et al., 2017). Deepwater oxygen renewal events occur primarily in later summer and fall, when dense oxygenated water accumulates outside of the fjord and periodically flows over the sill and into the basin (Anderson & Devol, 1973; Manning et al., 2010). These features make Saanich Inlet an ideal natural laboratory to examine the effects of dissolved oxygen availability on nitrogen cycling (Bourbonnais et al., 2013; Grundle & Juniper, 2011; Ward & Kilpatrick, 1990), greenhouse gas fluxes (Capelle et al., 2018, 2019), and microbial community dynamics (Torres-Beltrán et al., 2016; Zaikova et al., 2010). The detailed biogeochemical characterizations of Saanich Inlet provide a foundation for further exploration of N_2O production pathways and the regulating environmental factors, which have not been reported. In this study, we have built upon earlier nitrogen cycling studies by conducting ^{15}N tracer incubation experiments to directly measure N_2O production via multiple pathways along vertical and temporal oxygen gradients. The analyses of natural abundance bulk N_2O isotopes (^{15}N versus ^{14}N and ^{18}O versus ^{16}O) and isotopomers (the intramolecular configuration of nitrogen isotopes within the linear N_2O molecule) provide a further indication of how the different metabolic pathways have contributed to total N_2O production in Saanich Inlet. For example, ^{15}N tracer experiments determine potential and instantaneous N_2O production rates and pathways (Ji et al., 2018), whereas N_2O isotopomeric measurements reveal the dominant N_2O production pathway integrated over the history of a water mass (Fujii et al., 2013). The isotope measurements reported here were conducted on a recently developed laser-based analytical system that is able to deliver accuracy and precision comparable to traditional isotope ratio mass spectrometer techniques (Ji & Grundle, 2019). This work combines ^{15}N tracer incubation, N_2O concentration, and natural abundance isotopic/isotopomeric measurements to (1) elucidate the N_2O dynamics in a model coastal marine system with temporal and vertical oxygen gradients, (2) examine oxygen regulation of N_2O production pathways during bottle incubations and under in situ conditions, and (3) identify the major N_2O production pathways potentially contributing to atmospheric emissions.

2. Materials and Methods

2.1. Field Sampling

Four cruises were conducted on the *MSV John Strickland* in 2018 to conduct sampling in Saanich Inlet. Our sampling site (48°38.58′N, 123°29.93′W, depth 206 m, Figure S1) was ~10 km south of the inlet's mouth and ~5 km north of the monthly N_2O time series station reported by Capelle et al. (2018). Bimonthly sampling was conducted on 5 April, 14 June, 2 August, and 25 October 2018 to represent the transition from stable water column stratification and bottom water anoxia to deepwater oxygen renewal.

Six discrete sampling depths below the euphotic zone (75, 90, 100, 110, 130, and 160 m) were chosen to bracket the oxycline and were maintained consistently throughout the four cruises. Water samples were collected from 5-L Niskin bottles on a rosette sampler equipped with a conductivity-temperature-depth (CTD) package (SBE 19, Sea-Bird Electronics, Bellevue, WA). The CTD rosette was also equipped with an oxygen sensor (SBE 43, Sea-Bird Electronics) for real time, continuous profiling of DOs. Dissolved oxygen was also measured in discrete samples, using the Carpenter-Winkler titration method (Carpenter, 1965) for the purpose of calibrating the oxygen sensor. The discrete DO measurements generally had a reproducibility of 2% of mean values, and the oxygen sensor had a detection limit of ~2.5 μmol L^{-1}. We operationally define the terms *anoxic* as DO ranging from 0 to 2.5 μmol L^{-1}, *suboxic* as 2.5 to 15 μmol L^{-1}, and *oxygenated* as greater 15 μmol L^{-1}. It should be noted that at anoxic conditions (DO = 0–2.5 μmol L^{-1}), denitrification and sulfate reduction are probably the dominant microbial metabolism, yet oxygen respiration continues to operate even at nanomolar DO level (Zakem & Follows, 2017). And thus, denitrification, sulfate reduction and

oxygen respiration coexist at suboxic depths in Saanich Inlet (Bourbonnais et al., 2013; Manning et al., 2010; Torres-Beltrán et al., 2016). Seawater subsamples for nutrient measurements were filtered (0.22-μm Sterivex™ filter, EMD Millipore, Burlington, MA) and stored at −20 °C in acid-washed 60-ml high-density polyethylene bottles (20,160,060, Thermo Scientific, Waltham, MA, USA).

Duplicate samples for N_2O concentration measurements were filled from 5-L Niskin bottles into the bottom of 20-ml glass serum vials (LPP.10732, LEAP PAL Parts, Raleigh, NC, United States) and then were allowed to overflow at least three times the volume before sealing the vials with butyl septa (60180744, Thermo Scientific) and aluminum rings (60180512, Thermo Scientific). The mean volume of a crimp-sealed vial was 20.3 ± 0.06 ml. Duplicate samples for N_2O isotope and isotopomer measurements were crimp sealed in 60-ml glass serum bottles (223745, Wheaton, Millville, New Jersey, United States). Both concentration and isotope/isotopomer samples were immediately preserved with 0.05 ml of saturated mercuric chloride solution ($HgCl_2$). Samples were stored in the dark at 20 to 23 °C for less than 4 months before laboratory analyses (described in section 2.3).

2.2. Nitrogen Tracer Experiments

For N_2O production experiments, seawater was sampled from 5-L Niskin bottles into crimp-sealed 20-ml vials using the same technique as described for the N_2O concentration samples. To facilitate tracer addition, a 1-ml N_2 headspace was created in the crimp-sealed vials. During the October sampling, the four shallower depths (75, 90, 100, and 110 m) were treated with an air headspace to maintain oxygenated conditions. Final DOs in the water phase were calculated using equilibrium concentrations between the water and gas phases in the incubation vials (Garcia & Gordon, 1992) and were later confirmed by laboratory oxygen sensor measurements in a similar experimental setup (see supporting information Text S1). The water phase DO in vials with an N_2 headspace was approximately 40% of in situ concentration, whereas air headspace vials had elevated DO ranging from 187 to 210 μmol L^{-1}, in comparison to in situ DO of 43–101 μmol L^{-1} (see supporting information Table S1 for DO of all incubation experiments). Incubation experiments with ^{15}N tracers were applied to quantify rates of N_2O production from NH_4^+ oxidation, NO_2^-, and NO_3^- reduction. Three suites of ^{15}N tracer solutions ($^{15}NH_4^+$ plus $^{14}NO_2^-$, $^{15}NO_2^-$ plus $^{14}NH_4^+$, $^{15}NO_3^-$ plus $^{14}NH_4^+$, and $^{14}NO_2^-$, Sigma-Aldrich, St. Louis, Missouri, United States) were applied to enrich $^{15}NH_4^+$, $^{15}NO_2^-$, and $^{15}NO_3^-$ to 0.5, 0.5 and 1.0 μmol L^{-1} (final concentration, tracer ^{15}N atom % = 99%), respectively, and increased concentrations of $^{14}NH_4^+$, $^{14}NO_2^-$, or $^{14}NO_3^-$ by 0.5, 0.5, and 1.0 μmol L^{-1}, respectively. Tracers were dissolved in deionized water, and the solutions were flushed with N_2 before adding 0.1 ml into each vial. The set of incubations with $^{15}NH_4^+$ plus $^{14}NO_2^-$ was also used for measuring nitrification rates (oxidation of NH_4^+ to NO_2^- and NO_3^-), which allowed us to estimate the yield of N_2O from nitrification, defined as the molar nitrogen ratio of N_2O production to NH_4^+ oxidation (see section 3.4). Incubations lasted 12 to 18 hr in temperature-controlled chambers (±1 °C of in situ temperature), during which duplicate samples were preserved every 6 to 9 hr (3 time points in total) with 0.05 ml of saturated $HgCl_2$ solution. Preserved samples were stored in the dark at 20 to 23 °C for less than 4 months before performing N_2O isotopic/isotopomeric analyses (see section 2.3).

2.3. Laboratory Analyses

Concentrations of dissolved inorganic nitrogen species (NH_4^+, NO_2^- and NO_3^-) were determined as follows: NH_4^+ was measured fluorometrically by reaction with orthophthaldialdehyde (Holmes et al., 1999), with a detection limit of 0.02 μmol L^{-1}; NO_2^- was treated with the Griess reagent and measured colorimetrically (Hansen & Koroleff, 1999), with a detection limit of 0.005 μmol L^{-1} (using a 10-cm cuvette); and $NO_3^- + NO_2^-$ was measured using the cadmium reduction method (Hansen & Koroleff, 1999), with a detection limit of 0.02 μmol L^{-1}. Although not experimentally measured, the presence of hydrogen sulfide (H_2S) was indicated by its recognizable smell. However, samples for nutrient analyses were filtered in open air, and H_2S was probably oxidized. It is therefore unlikely for H_2S to have interfered with $NO_3^- + NO_2^-$ measurements.

Analyses of N_2O concentration and isotope/isotopomer ratios were performed using a purge-and-trap module coupled to a cavity ring-down spectrometer (PT-CRDS) recently developed in the Grundle Laboratory. The PT-CRDS is an automated, laser-based system that provides comparable accuracy and precision to gas chromatography and isotope ratio mass spectrometer techniques for N_2O concentration and

isotope/isotopomer ratio measurements, respectively. A full description of this technique is outlined in Ji and Grundle (2019). Isotopic analysis determines the relative abundances of nitrogen isotopes ($\delta^{15}N_{bulk}$) and oxygen isotopes ($\delta^{18}O$) of the entire N_2O pool, whereas isotopomeric analysis discerns the intramolecular nitrogen isotope substitution (isotopomers) on the linear asymmetric N_2O molecule (N = N = O). By convention, the relative abundance of ^{15}N substitutions of the central ($^{14}N = {}^{15}N = {}^{16}O$) and terminal positions ($^{15}N = {}^{14}N = {}^{16}O$) are denoted as $\delta^{15}N_2O_\alpha$ and $\delta^{15}N_2O_\beta$, respectively. Briefly, the PT-CRDS analyses employed the following methodology: Dissolved N_2O in sample vials was extracted by N_2 purging and cryotrapped using liquid nitrogen at working temperature of 130 ± 10 K (note that N_2O boiling temperature is 185 K). Heating to 480 K released the gaseous N_2O, after which concentrations and isotope/isotopomer ratios were measured by quantitative light dissipation at specific wavelengths ($^{14}N = {}^{15}N = {}^{16}O$, $^{15}N = {}^{14}N = {}^{16}O$, and $^{14}N = {}^{14}N = {}^{18}O$ at 2195.76195, 2198.79576, and 2195.95102 cm^{-1}, respectively). Raw isotopic measurements were corrected for sample size-dependent isotopic deviations caused by varying N_2O concentrations (Ji & Grundle, 2019) and calibrated with isotopic reference materials (see Table S2). Because the optimal quantity of N_2O for highly accurate isotopic/isotopomeric analyses by PT-CRDS is 0.5–0.8 nmol-N_2O, samples from 130 and 160 m in April and 160 m samples in June did not contain enough N_2O, and, as such, those results are not reported.

The $^{15}NH_4^+$ incubation set was used for quantifying nitrification rates after measuring $\delta^{15}N$-N_2O. Nitrification rates were determined as the transfer of nitrogen from NH_4^+ to NO_2^- + NO_3^- (Laperriere et al., 2019). The $\delta^{15}N$ signature of NO_2^- + NO_3^- ($\delta^{15}_{NO_x^-}$) was measured using the same PT-CRDS technique outlined above, but only after first converting the NO_2^- + NO_3^- to N_2O in crimp-sealed 20-ml vials using the denitrifier method (Weigand et al., 2016). A set of 20-ml vials (LPP.10732, LEAP PAL Parts, Raleigh, NC, United States) containing live bacterial concentrate *Pseudomonas chlororaphis* (ATCC® 43928™, Manassas, Virginia) in buffer solution (pH = ~7.3) were purged with nitrogen gas to create anaerobic conditions in the vials. The water samples were treated with 0.05 ml of 10 mol L^{-1} sodium hydroxide solution in order to precipitate mercury; the supernatant was transferred to the bacterial vials for complete conversion of NO_2^- + NO_3^- to N_2O within 3 hr of incubation at 22 °C. As the NO_2^- + NO_3^- concentrations of water samples ranged from 0.6 to 32 μmol L^{-1}, the volume of water sample injected for bacterial conversion was adjusted to accommodate 0.5 nmol-N_2O in order to achieve accurate $\delta^{15}N$ measurements by the PT-CRDS. To calibrate the measurements, isotopic reference vials were prepared by bacterial conversion of potassium nitrate USGS-35 ($\delta^{15}N$ = 2.7‰ versus Air N_2) and USGS-32 ($\delta^{15}N$ = 180‰ versus Air N_2).

2.4. Data Processing

Water column N_2O saturation was quantified by the N_2O excess (ΔN_2O), defined as the concentration difference between measured and equilibrium values with respect to the atmosphere.

$$\Delta N_2O = [N_2O]_{measured} - [N_2O]_{equilibrium} \quad (1)$$

Equilibrium N_2O concentrations are temperature and salinity dependent and were calculated according to Weiss and Price (1980) using atmospheric N_2O concentration of 330 ppb.

The δ notation is used to quantify the relative abundance of N_2O isotopomers (Coplen, 2011) in Equations 2 and 3.

$$\delta^{15}N_2O_\alpha = \frac{\left(^{14}N^{15}N^{16}O/{}^{14}N^{14}N^{16}O\right)}{R_{ref}} - 1, \quad R_{ref} = \frac{^{15}N}{^{14}N} \text{ of atmospheric } N_2, \text{ 0.003667} \quad (2)$$

$$\delta^{15}N_2O_\beta = \frac{\left(^{15}N^{14}N^{16}O/{}^{14}N^{14}N^{16}O\right)}{R_{ref}} - 1, \quad R_{ref} = \frac{^{15}N}{^{14}N} \text{ of atmospheric } N_2, \text{ 0.003667} \quad (3)$$

The bulk isotopes of N_2O are defined in Equations 4 and 5.

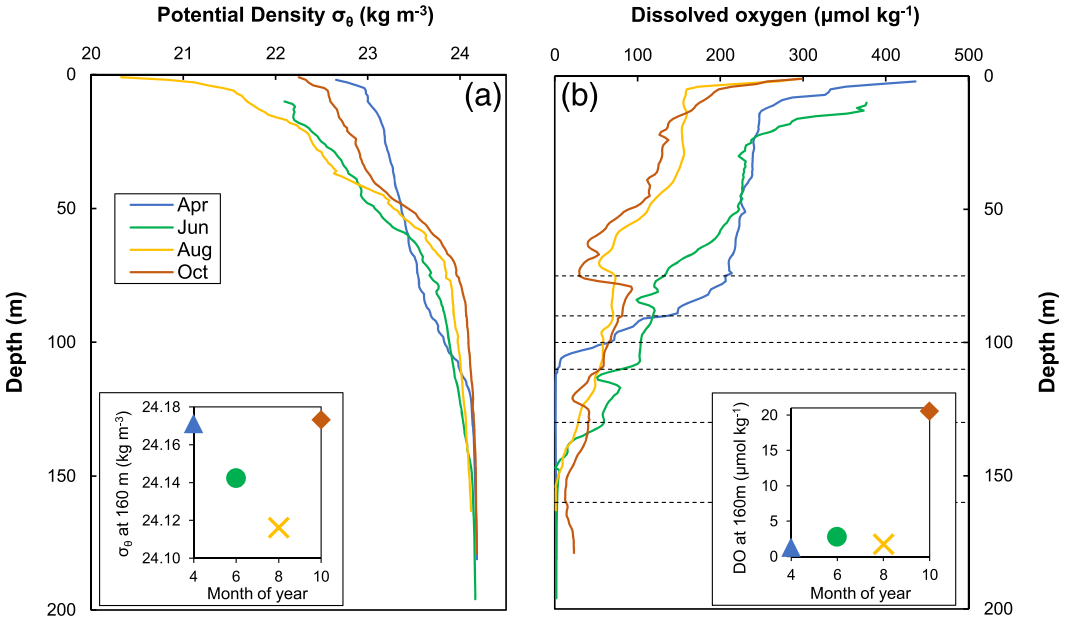

Figure 1. Profiles of water column (a) potential density and (b) dissolved oxygen at the sampling station in Saanich Inlet (48°47.707′N, 123°29.927′W) during four campaigns in 2018 (April, June, August, and October). Inset figures of (a) and (b) show the potential density and dissolved oxygen at 160 m. Dashed lines in (b) indicate the sampling depths (75, 90, 100, 110, 130, and 160 m) for inorganic nitrogen analyses and N_2O production experiments.

$$\delta^{18}\text{O-N}_2\text{O} = \frac{(^{18}\text{O}/^{16}\text{O})}{R_{ref}} - 1, \quad R_{ref} = \frac{^{18}\text{O}}{^{16}\text{O}} \text{of VSMOW, } 0.002005 \tag{4}$$

$$\delta^{15}\text{N}_{\text{bulk}}\text{-N}_2\text{O} = \frac{\delta^{15}\text{N}_\alpha + \delta^{15}\text{N}_\beta}{2} \tag{5}$$

Site preference (SP) quantifies the relative abundance of the two N_2O isotopomers according to Equation 6.

$$\text{SP} = \delta^{15}\text{N}_\alpha - \delta^{15}\text{N}_\beta \tag{6}$$

The N_2O production rate R_{N2O} (nmol-N L^{-1} day^{-1}) is calculated according to Equation 7

$$R_{N_2O} = 2 \times \frac{d(^{15}\text{N}_2\text{O})/\text{d}t}{F} \tag{7}$$

where $^{15}N_2O$ represents concentration of ^{15}N-labeled N_2O molecules, $d^{15}N_2O/dt$ represents the slope of the linear regression of $^{15}N_2O$ against time, and F represents ^{15}N enrichment of substrate (2–99% at different depths). The conversion of $\delta^{15}N_{bulk}$-N_2O to $^{15}N_2O$ is calculated according to Equation 8

$$^{15}\text{N}_2\text{O} = [\text{N}_2\text{O}] \times \frac{\left(\delta^{15}\text{N}_{bulk}\text{-N}_2\text{O} + 1\right) \times R_{ref}}{1 + \left(\delta^{15}\text{N}_{bulk}\text{-N}_2\text{O} + 1\right) \times R_{ref}} \tag{8}$$

where $[N_2O]$ is the concentration of N_2O during the incubation experiments and $R_{ref} = 0.003667$. The detection limit of rate measurement was 0.002 nmol-N L^{-1} day^{-1}.

Calculation of nitrification rate R_{nit} is according to Laperriere et al. (2019)

$$R_{nit} = \frac{\text{d}\left(^{15}\text{NO}_x^-\right)/\text{d}t}{F^{15}_{\text{NH}_4^+}} \tag{9}$$

where $d^{15}NO_x^-/dt$ represents the slope of linear regression of ^{15}N atom % of NO_3^- + NO_2^- (abbreviated as

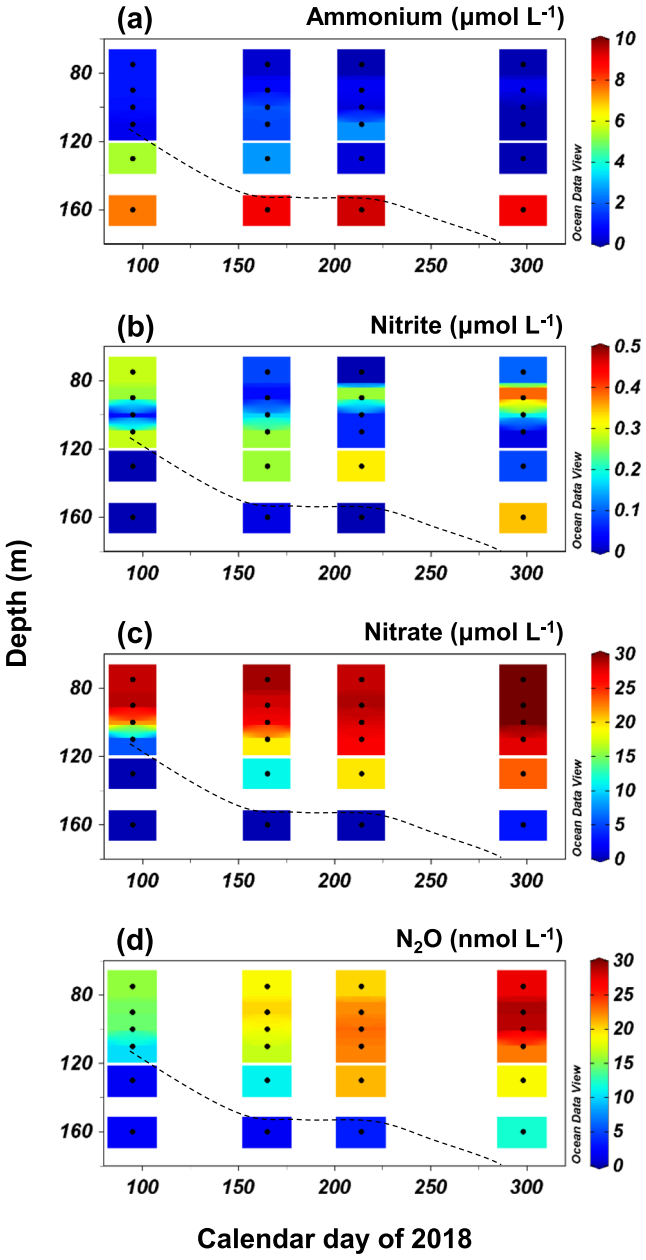

Figure 2. Concentration profiles of (a) ammonium, (b) nitrite, (c) nitrate, and (d) nitrous oxide at the sampling station (48°47.707′N, 123°29.927′W) during four sampling campaigns. Dashed line marks the approximate position of the oxic-anoxic interface (dissolved oxygen concentration = 2.5 μmol L^{-1} isoline).

NO_x^-) on time and $F^{15}_{NH_4^+}$ represents ^{15}N fraction labeled of substrate ammonium (5–99%). The value of $^{15}NO_x^-$ is calculated according to Equation 10

$$^{15}NO_x^- = [NO_x^-] \times \frac{\left(\frac{\delta^{15}_{NO_x^-}}{1000}+1\right) \times R_{ref}}{1+\left(\frac{\delta^{15}_{NO_x^-}}{1000}+1\right) \times R_{ref}} \quad (10)$$

where $[NO_x^-]$ is the concentration of NO_3^- + NO_2^- during the incubation experiments and $\delta^{15}_{NO_x^-}$ is the $\delta^{15}N$ signature of NO_x^- measured by denitrifier method.

The nitrification N_2O yield is defined as the molar nitrogen ratio of N_2O versus nitrification. Two independent estimates of the N_2O yield are presented. First is the *rate ratio yield*, which is the ratio of directly measured rates of N_2O production versus nitrification during $^{15}NH_4^+$ incubations, and it reveals instantaneous yield from bottle incubations at a range of oxygen levels. Note that oxygen concentrations in the incubation vials were different from those in situ levels (see section 2.2). Second is the *regression yield* using the nitrate-ΔN_2O relationship, which is based on by-production of N_2O during NH_4^+ oxidation to NO_3^- in oxygenated waters below the euphotic zone, assuming stoichiometric conversion (i.e., 1 mol NH_4^+:1 mol NO_3^-) and negligible accumulation of NO_2^- (Grundle et al., 2012; Rees et al., 2011). Such an indirect estimate reveals temporal- and spatial-averaged N_2O yield inside Saanich Inlet. To accurately characterize nitrate-ΔN_2O relationship during remineralization inside Saanich Inlet, we used NO_3^- and ΔN_2O measurements from this study and a 9-year time series data set at 40–150 m depth from a nearby station in Saanich Inlet (Torres-Beltrán et al., 2017).

3. Results

3.1. Water Column Structure and Chemistry

The water column potential density in Saanich Inlet ranged from 20.2 to 24.2 kg m^{-3}. From April to August, a progressive decrease in density of the upper 50 m signaled increased stratification. The October water column had increased density in comparison to August. At 160 m, the density level of October was similar to that of April (Figure 1a). The DOs in the upper 10 m were high and often supersaturated (up to 140%). From April to August, in situ DO decreased with depth, with anoxic conditions persisting below 110 m in April and below 150 m in June and August (Figure 1b). The 160-m water samples from April, June, and August as well as 130 m from April exhibited recognizable H_2S odor, thus providing anecdotal evidence of its presence (H_2S was not measured here), and substantiated the anoxic conditions at these depths. In October, the entire water column was oxygenated (DO > 20 μmol L^{-1}, Figure 1b), indicating the progressive deepening of oxic-anoxic interface (DO = 2.5 μmol L^{-1} isoline) from April to October. Based on data from Ocean Networks Canada sensor platforms in Saanich Inlet (data not shown), oxygen renewal events appeared to have occurred in late August and mid-October. During these renewal events, dense and oxygenated water replaced the deep water inside the basin, increasing density and DO at 160 m (Figures 1a and 1b).

Inorganic nitrogen species (NH_4^+, NO_2^-, and NO_3^-) distributed differently along the oxycline. In shallower oxygenated waters, NH_4^+ concentrations were generally ~1.0 μmol L^{-1}. Higher NH_4^+ concentrations (5–

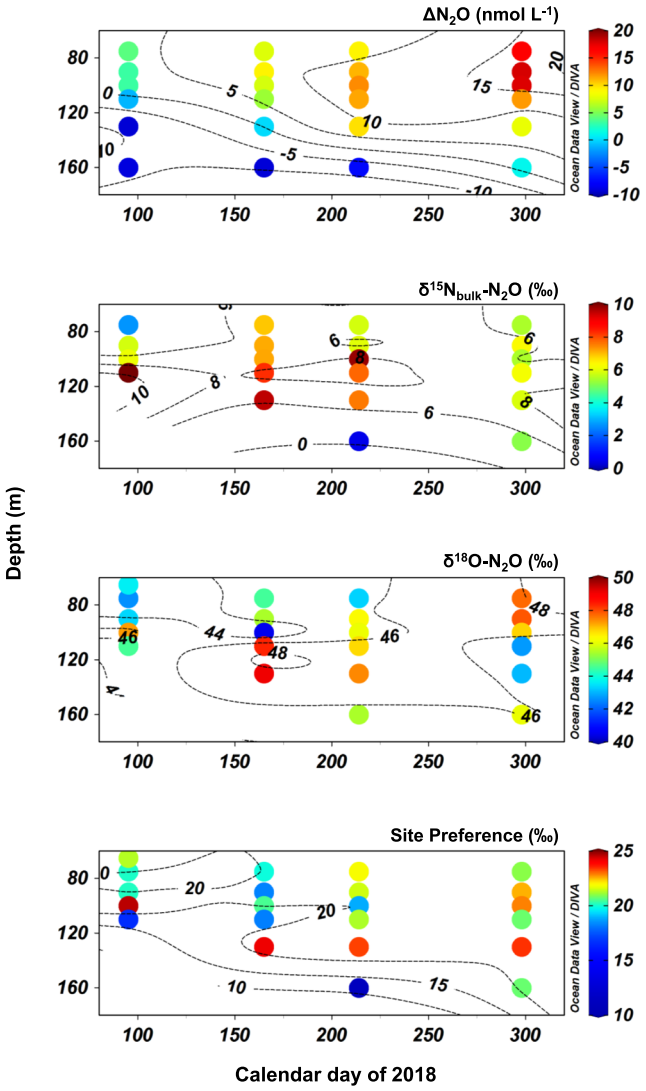

Figure 3. Water column profiles of (a) N_2O supersaturation (ΔN_2O), (b) $\delta^{15}N_{bulk}$-N_2O, (c) $\delta^{18}O$-N_2O, and (d) site preference at the sampling station. Contour lines were extrapolated using DIVA algorithm from Ocean Data View software.

10 μmol L^{-1}) occurred in deeper anoxic waters, that is, below 130 m in April and at 160 m in June and August (Figure 2a). Nitrite concentrations were generally low (<0.5 μmol L^{-1}) throughout the water column for all sampling dates. Local NO_2^- maximum concentrations (~0.3 μmol L^{-1}) occurred above the oxic-anoxic interface (Figure 2b). The concentrations of NO_2^- were below detection at the anoxic depths. The distribution of NO_3^- showed a somewhat opposite distribution to that of NH_4^+. In oxygenated waters between 75 and 100 m, NO_3^- concentrations were 25–30 μmol L^{-1}; the concentrations decreased markedly at deeper depths, coinciding with an increase of NO_2^- above the oxic-anoxic interface (Figure 2c). Very low NO_3^- concentrations (< 0.2 μmol L^{-1}) occurred in deep anoxic waters.

3.2. Nitrous Oxide Concentration and Isotopes

Water column N_2O concentrations were 10–29 nmol L^{-1} above the oxic-anoxic interface and decreased with depth. From April to October, N_2O concentrations at oxycline depths (75–110 m) progressively increased (Figure 2d). Supersaturations of N_2O (ΔN_2O up to 20 nmol L^{-1}) were observed at shallower oxycline depths from April to October (Figure 3a). Within the anoxic depths in April, June, and August, pronounced N_2O undersaturation (ΔN_2O ranged from −7.7 to −9.3 nmol L^{-1}) was observed. From August to October, N_2O concentrations at 160 m increased to near equilibrium concentration (ΔN_2O = 1 nmol L^{-1}). The oxygenated and suboxic depths had variable $\delta^{15}N_{bulk}$-N_2O values ranging from 5‰ to 10‰ (Figure 3b) and $\delta^{18}O$-N_2O 40‰ to 49‰ (Figure 3c). SP values were 15–25‰ and generally increased with depth and with decreasing DO (Figure 3d). The only isotope/isotopomer sample from the anoxic depths was at 160 m in August, where the values of $\delta^{15}N_{bulk}$-N_2O, $\delta^{18}O$-N_2O, and SP were 0.4‰, 45‰, and 11‰, respectively.

3.3. Nitrous Oxide Production Pathways

Production of N_2O from NH_4^+ oxidation occurred in the oxygenated and suboxic waters, coinciding with positive ΔN_2O concentrations. In April, June, and August, rates of N_2O production peaked at 100–110 m (Figures 4a–4c) where in situ DO was 50–80 μmol L^{-1}. The maximum rate of N_2O production from NH_4^+ oxidation was much higher in April (0.35 nmol-N L^{-1} day^{-1}) than those in June and August (~0.05 nmol-N L^{-1} day^{-1}). No production of N_2O from NH_4^+ oxidation was detected at 130 m and below in April and at 160 m in June. In August, NH_4^+ oxidation to N_2O was detected at 160 m despite anoxic conditions (Figure 4c). In October following the renewal event, all sampling depths showed N_2O production from NH_4^+ oxidation, and the rates increased with depth. At 160 m where in situ DO was 21 μmol L^{-1}, a maximum rate of N_2O production from NH_4^+ oxidation was reached at ~1 nmol-N L^{-1} day^{-1} (Figure 4d), 3 to 25 times the maximum rates in April, June, and August.

Production of N_2O from NO_2^- reduction and NO_3^- reduction occurred at suboxic and anoxic conditions. Highest rates of N_2O production from NO_2^- reduction and NO_3^- reduction occurred at the oxic-anoxic interface, at 110 m in April (Figure 4e) and at 160 m in June and August (Figures 4f and 4g). These depths had pronounced N_2O undersaturation (Figure 3a) and low NO_2^- and NO_3^- concentrations that were close to the detection limit (Figures 2b and 2c). In October, low rates of N_2O production from NO_2^- and NO_3^- reduction were detected (<0.09 nmol-N L^{-1} day^{-1}, Figure 4h); these rates generally increased with depth and with decreasing DO.

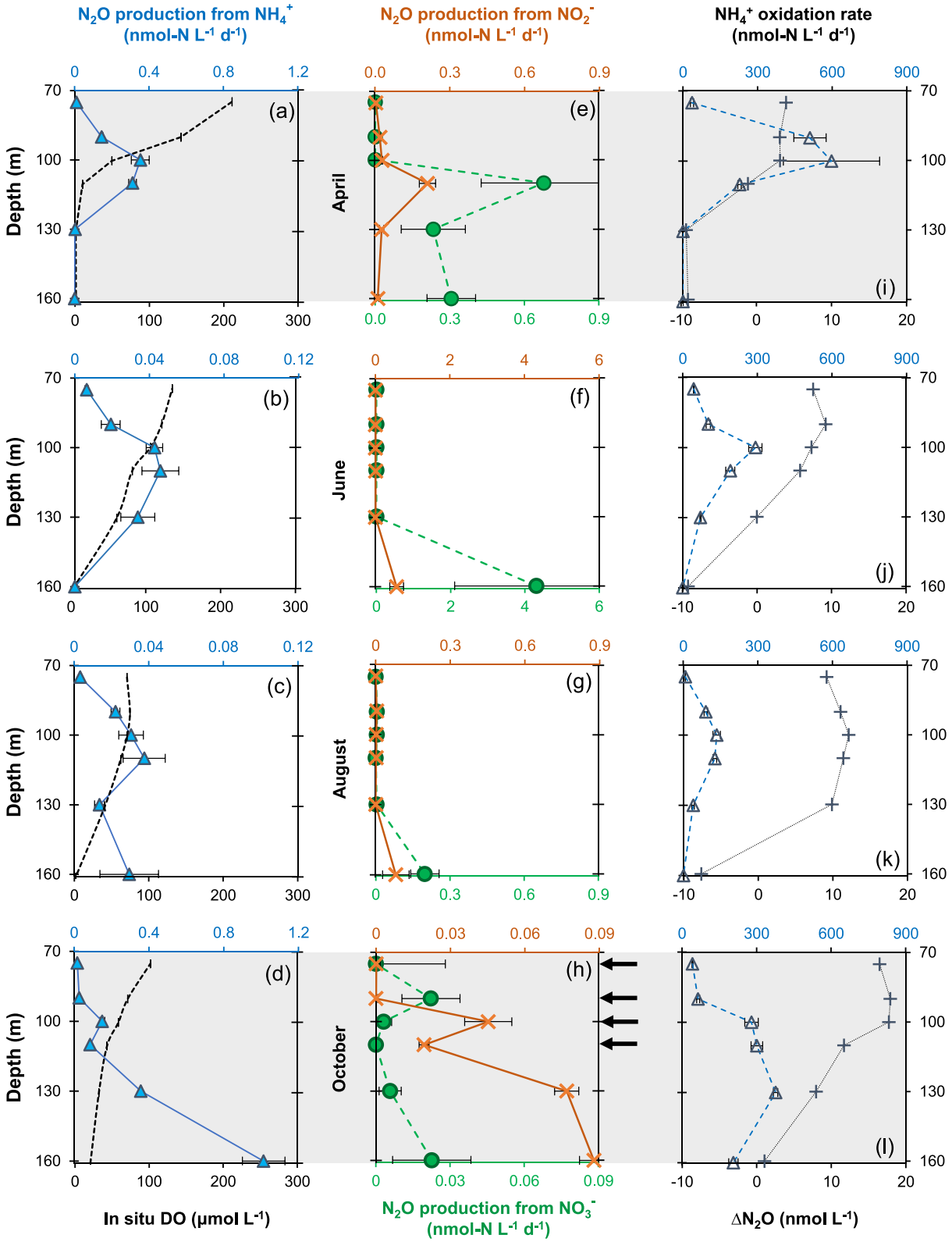

Figure 4. Profiles of N_2O production rates, nitrification rates, and corresponding dissolved oxygen concentrations. (a–d) N_2O production from NH_4^+ oxidation (triangle) and dissolved oxygen profile (dashed line). (e–h) N_2O production from NO_2^- (cross) and NO_3^- reduction (circle). (i–l) Nitrification rate (triangle) and ΔN_2O concentrations (plus sign) during four sampling campaigns (a, e, and i: April; b, f, and j: June; c, g, and k: August; d, h, and l: October). Arrows in (h) indicate that rate measurements were conducted under air headspace, thus having DO = 180–210 μmol L^{-1}, whereas the rest of the incubations were conducted under N_2 headspace, having dissolved oxygen about 40% of in situ levels (see Table S1).

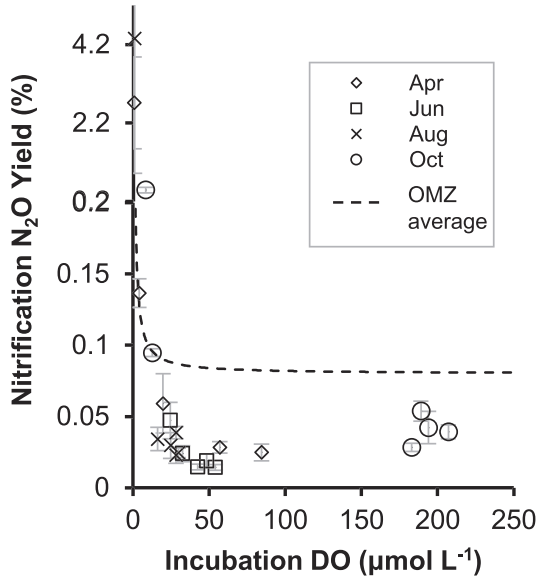

Figure 5. N_2O yield during NH_4^+ oxidation in Saanich Inlet, measured as rate ratios of N_2O production versus NH_4^+ oxidation by ^{15}N incubation experiments (referred to as *rate ratio yield*) during sampling in April (diamonds), June (squares), August (crosses), and October (circles). Dashed line represents the average yield reported by Ji et al. (2018) for the eastern tropical South and North Pacific oxygen minimum zones. Note that the scale on *y* axis is nonlinear.

3.4. Nitrification and Nitrous Oxide Yield

Nitrification (measured as NH_4^+ oxidation to NO_2^- plus NO_3^-) occurred in oxygenated and suboxic zones (DO > 2.5 μmol L^{-1}) from April to October. Both shallow (<90 m) and deep (160 m) layers had lower rates, while the highest rates often occurred at suboxic depths close to the oxic-anoxic interface (Figures 4i–4l). Maximum rates were 130–600 nmol-N L^{-1} day^{-1} at in situ DO = 30–140 μmol L^{-1} from April to October. Nitrification was not detected at 160 m in April and June, and rates were comparably low at 130 m in April (0.08 nmol-N L^{-1} day^{-1}, Figure 4i) and at 160 m in August (0.68 nmol-N L^{-1} day^{-1}, Figure 4l). Two independent estimates of N_2O yield during nitrification are compared as follows. The rate ratio yield ranged from 0.014 to 0.059% at DO = 15–210 μmol L^{-1} during bottle incubations and increased significantly to 4.3 ± 3.4% at DO < 1 μmol L^{-1} in a nonlinear fashion (Figure 5). Using nitrate concentration and ΔN_2O data in this study and from time series observations from Torres-Beltrán et al. (2017), the regression yield was 0.045 ± 0.006%, which is within the range of the rate ratio yield from direct measurements at DO > 15 μmol L^{-1} (0.014–0.059%).

4. Discussion

Saanich Inlet is a model coastal system with vertical and temporal gradients of oxygen and inorganic nitrogen that can be ideal for investigating N_2O dynamics. Incubation experiments with ^{15}N-labeled substrates directly measured the rates of N_2O production via NH_4^+ oxidation, NO_2^- reduction, and NO_3^- reduction under variable DO gradients. This allows for an objective assessment of the relative contributions of oxidative and reductive N_2O production pathways, as well as the regulatory effects of DO. Evidently, NH_4^+ oxidation was the dominant N_2O production pathway throughout our sampling period under oxygenated conditions (DO > 15 μmol L^{-1}, Figure 6a). Incubation experiments demonstrating potential N_2O production rates from the oxycline to anoxic depths are important for interpreting temporal and vertical ΔN_2O profiles. Samples with positive ΔN_2O concentrations generally co-occurred with higher rates of N_2O production via NH_4^+ oxidation than rates of NO_2^- and NO_3^- reduction (Figure 6b). Active NO_2^- and NO_3^- reduction to N_2O were mostly confined to suboxic and anoxic waters (DO < 15 μmol L^{-1}). Furthermore, N_2O was undersaturated at anoxic depths, indicating net N_2O consumption as a result of complete denitrification. Both NO_3^- and NO_2^- reduction to N_2O can be regarded as partial denitrification; however, it has been shown that the two pathways were performed independently by denitrifying cells, and intracellular exchange of NO_2^- was not detected (Ji et al., 2018). Thus, rates of NO_3^- and NO_2^- reduction to N_2O were measured separately, and it is unnecessary for the two sets of rates to match. Furthermore, these potential rates were detected at depths with near depletion of NO_2^- and NO_3^- (Figures 2b and 2c); thus, addition of ^{15}N-labeled NO_2^- and NO_3^- substrates could stimulate N_2O production via partial denitrification mediated by active denitrifying microbial communities (Capelle et al., 2018; Zaikova et al., 2010) capable of short-term response to inputs of electron acceptors.

As previously explained, ^{15}N incubation experiments were performed under altered DO, and this had minimal effect on determining the major N_2O production pathway in the water column. Potential microbial activities in the water column were demonstrated by these measured rates, which can be comparable provided that they were conducted under similar experimental conditions (e.g., comparable rates measured from N_2-headspace vials). For example, during incubation experiments in October, the 130 and 160 m samples had decreased DO with respect to in situ values (Table S1), which may have stimulated N_2O production from NH_4^+ oxidation. The oxycline samples (75–110 m) were treated with air headspace and had higher DO than in situ levels. While it is possible that N_2O production from NH_4^+ oxidation was inhibited by elevated DO (see section 3.3), these October samples from 75 to 110 m also showed higher rates (0.02–0.15 nmol-N L^{-1} day^{-1}) in comparison to August samples from the same depths, which were conducted under N_2

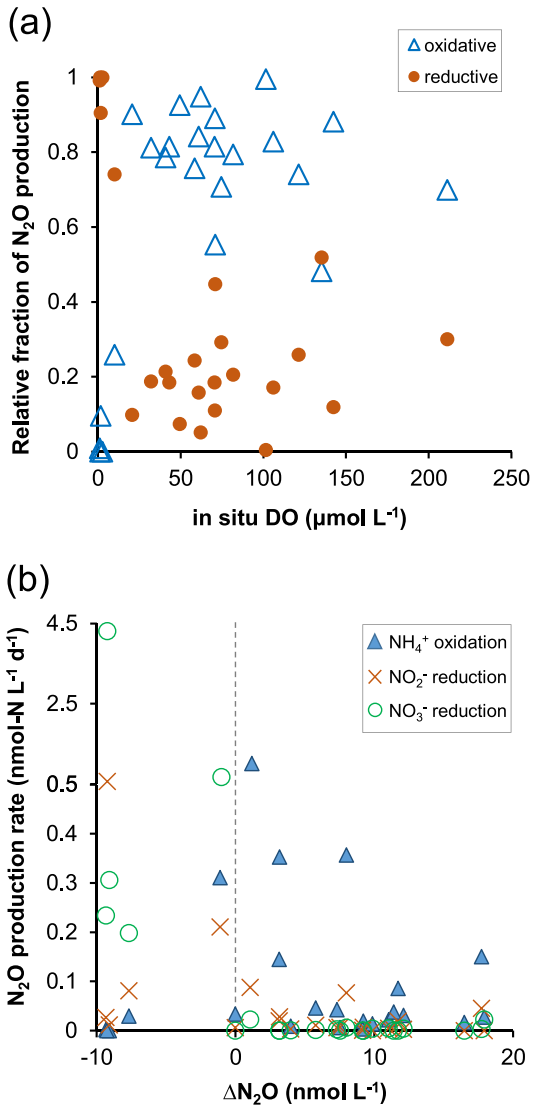

Figure 6. (a) The fraction of N_2O production from oxidative pathway (NH_4^+ oxidation, open triangle) and reductive pathway (NO_2^- + NO_3^- reduction, filled circle) plotted against in situ dissolved oxygen concentration. (b) Rates of N_2O production via NH_4^+ oxidation (triangle), NO_2^- reduction (cross), and NO_3^- reduction (circle) plotted against N_2O supersaturation (ΔN_2O). Dashed line marks saturated N_2O concentration with respect to atmosphere. Note that the scale on *y* axis is nonlinear.

headspace. Production of N_2O from NO_2^-/NO_3^- reduction could be overestimated because of lowered DO during the incubation experiments with N_2 headspace. Thus, the relative importance of partial denitrification to total N_2O production could be overestimated, further substantiating our conclusion that NH_4^+ oxidation was the dominant N_2O production pathway.

Two additional factors should be acknowledged when interpreting the rate measurements obtained from ^{15}N tracer incubations. (1) Variable in situ NH_4^+, NO_2^- and NO_3^- concentrations resulted in 2–99% ^{15}N enrichment of substrates at the start of incubations. Therefore, rate measurements of N_2O production from NH_4^+ oxidation (and nitrification) above 100 m depth and all of N_2O production from NO_2^- reduction and rates of NO_3^- reduction at 160 m (see section 3.3) should reflect microbial potential at these depths. (2) Dilution of ^{15}N tracers during incubation experiments results in underestimation of N_2O production rates. Variable dilution of $^{15}NO_2^-$ was estimated (0–27%) using nitrification rate measurements. Dilution effects for other sets of tracer additions ($^{15}NH_4^+$ and $^{15}NO_3^-$) were not estimated, and rates should be considered conservative.

The SP value of N_2O is not merely an index characterizing the relative abundance of $\delta^{15}N_2O_\alpha$ over $\delta^{15}N_2O_\beta$; it also provides an additional, independent constraint of N_2O production pathways with respect to ^{15}N incubation experiments. The SP value can also serve as a quantitative indicator for the fraction of N_2O produced via oxidative and reductive pathways. Microbial N_2O production via NH_4^+ oxidation and NO_2^- and/or NO_3^- reduction has SP values of 30 ± 5 ‰ and 0 ± 5‰, respectively, and these values are independent of substrate isotopic composition across a wide range of environments (Toyoda et al., 2017). During N_2O production, the N_2O isotopes and SP signatures follow mass conservation. The mass balance model proposed by Fujii et al. (2013) quantified the SP signature of N_2O produced ($SP_{produced}$) by the linear regression of the observed isotope values ($SP_{observed}$) on the inverse N_2O concentration ($1/[N_2O]_{measured}$). Saanich Inlet samples showed an $SP_{produced}$ value of 23 ± 0.6‰ (or 24 ± 1‰ without an outlier data point, Figure 7a), lending further support to NH_4^+ oxidation being the predominant N_2O production pathway. Here, ^{15}N tracer incubation experiments and natural abundance SP values permitted a parallel view of N_2O production pathways in bottle incubations in comparison to the predominant production pathways in situ. The fraction of N_2O produced via NH_4^+ oxidation determined by ^{15}N tracer experiments was plotted against SP values from the corresponding samples (Figure 7b). Higher contributions from NH_4^+ oxidation results in SP values close to 25‰, whereas higher contribution from reductive pathways results in SP values close to 10‰. These data can be explained by a mixing model with two end members: one with SP = 25 ± 5‰ representing N_2O production from NH_4^+ oxidation and the other with SP = 10 ± 5 ‰, respectively representing N_2O production from NO_2^- and/or NO_3^- reduction. Additional studies are needed to test the robustness of using SP signatures to quantitatively determine the fraction of N_2O produced via oxidative and reductive pathways in Saanich Inlet and elsewhere.

In all, the two independent methods, natural abundance isotopomers and ^{15}N tracer incubation experiments, delivered consistent results demonstrating that the dominant N_2O production pathway in Saanich Inlet is NH_4^+ oxidation. A notable difference between Saanich Inlet and open ocean OMZs is high NH_4^+

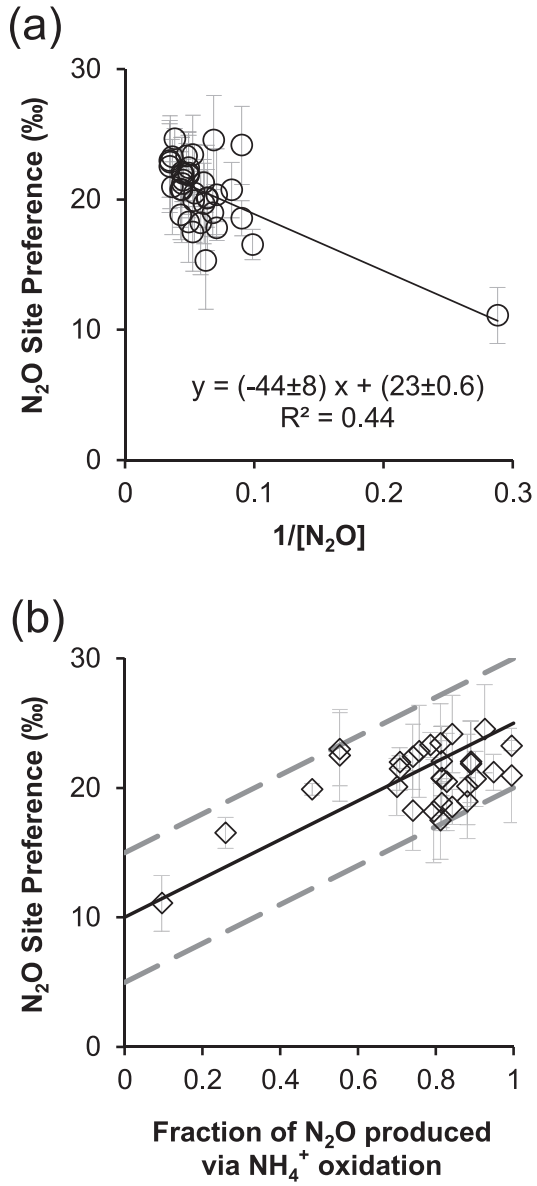

Figure 7. (a) Linear regression of N_2O site preference on inverse N_2O concentrations. Note: Without the outlier data point near the right edge of the plot, regression has a *y* intercept of 24 ± 1. (b) N_2O site preference (SP) measured in situ plotted against the fraction of N_2O production from NH_4^+ oxidation measured by ^{15}N incubation experiments. Solid line represents mixing between two end members, one with SP signature of 25 ‰ representing N_2O production from NH_4^+ oxidation and the other with SP signature of 10 ‰ representing N_2O production from NO_2^- or NO_3^- reduction. Two dashed lines represent upper and lower SP values of N_2O when mixing between NH_4^+ oxidation and NO_2^- or NO_3^- reduction having ±5‰ variation in their respective SP signatures.

fluxes generated by organic matter remineralization from the anoxic depth in Saanich Inlet (Bourbonnais et al., 2013). Using NH_4^+ concentration profiles from this study and assuming a diffusion constant of 1.0 m^2 day^{-1} previously estimated in Saanich Inlet 130–160 m depth (Louca et al., 2016), upward NH_4^+ fluxes from the anoxic zone ranged from 0.6 to 3.5 nmol m^{-2} s^{-1}. Such NH_4^+ fluxes are similar to the Black Sea water column with sulfidic bottom water (Fuchsman et al., 2008). Similarly, NH_4^+ oxidation was the dominant N_2O production pathway in the Black Sea (Westley et al., 2006).

Availability of oxygen is an important factor regulating N_2O yield during nitrification. Short-term DO changes (e.g., <3 hr) during incubation experiments can significantly change the yield (Ji et al., 2018; Löscher et al., 2012). In Saanich Inlet, the rate ratio yield increases with decreasing oxygen concentrations, particularly under suboxic conditions (DO < 15 μmol L^{-1}). Saanich Inlet samples had rate ratio yield values similar to open ocean OMZ averages at DO < 15 μmol L^{-1}; however, the yield values are generally lower than OMZ averages at DO > 15 μmol L^{-1} (Figure 5). To better estimate nitrification N_2O yield using nitrate-ΔN_2O relationship, we excluded NO_3^- and ΔN_2O data from the surface euphotic zone and deep anoxic layer and used measurements from this study and a 9-year time series data set at 40–150 m depth from a nearby station in Saanich Inlet (Torres-Beltrán et al., 2017), for two reasons: (1) Both NO_3^- and ΔN_2O can be transported into Saanich Inlet by renewal water, which can alter the nitrate-ΔN_2O relationship especially for samples at depths below 160 m (Anderson & Devol, 1973; Capelle et al., 2018). As such, N_2O yield estimates could be altered by signals outside the inlet. (2) Both phytoplankton activity in the euphotic zone (Grundle et al., 2009) and nitrogen loss processes in the anoxic layer (Bourbonnais et al., 2013) decrease surface and bottom water NO_3^-, respectively. Using the nitrate-ΔN_2O relationship to infer regression yield across wider range of oxygen levels at various marine environments (Table 1), we found that yields in Saanich Inlet were, on average, lower than those from open-ocean OMZs influenced by coastal upwelling (e.g., the Eastern tropical South Pacific) and similar to those from oxygenated oceans (e.g., Subarctic region of Pacific and Atlantic). Furthermore, a proxy of N_2O yield during nitrification is the regression slope of ΔN_2O-AOU relationship; compilation of ΔN_2O versus AOU also showed Saanich Inlet to have lower ratios of ΔN_2O versus AOU than those of open-ocean OMZs (Capelle et al., 2018; Grundle et al., 2012). Thus, we conclude that Saanich Inlet samples displayed lower N_2O yields, particularly at oxygenated conditions (DO > 15 μmol L^{-1}) than those observed in open-ocean OMZs.

As a microbial process, N_2O production from NH_4^+ oxidation is mediated by two distinct microbial groups, ammonium oxidizing archaea (AOA) and ammonium oxidizing bacteria (AOB). Ammonia oxidizers can be found close to the oxic-anoxic interface and can utilize nanomolar oxygen level (Bristow et al., 2016; Louca et al., 2016), which can explain the detection of nitrifying activity at 130 m in April and at 160 m in August (section 3.4). In the open ocean, the ammonia oxidizing community is dominated by AOA (Horak et al., 2018), which have been shown to demonstrate higher N_2O yields than AOB (Löscher et al., 2012), and AOA is largely responsible for N_2O production (Santoro et al., 2011). In coastal zones, the relative abundance of AOB was shown to

Table 1
Nitrification N_2O Yield Indicated by Nitrate-ΔN_2O Relationship (Referred to as Regression Yield) at Various Marine Environments

Sampling location	N_2O Yield (%)	O_2 (μmol L^{-1})	Depth (m)	Data source
Saanich Inlet	0.039–0.051	0–226	40–150	This study and Torres-Beltrán et al. (2017)
Eastern tropical South Pacific	0.169–0.851	20–230	5–500	Ji et al. (2019)
Mauritanian upwelling	0.130–0.257	>35	0–2930	Rees et al. (2011)
Northeast Pacific	0.08	16–342	0–600	Grundle et al. (2012)
Subarctic North Atlantic	0.057 – 0.077	210–290	20–1000	Ji and Ward (2017)

Note. See regression plots in Figures S2a and S2b, respectively.

increase with increasing DO along the oxycline (Santoro et al., 2008). In contrast, N_2O yields from ammonium oxidation under suboxic conditions (DO < 15 μmol L^{-1}) in Saanich Inlet were similar to those under open ocean suboxic conditions. This similarity may indicate that the relative importance of AOA versus AOB is more comparable between coastal and open-ocean systems when suboxic conditions persist. Further analyses of the relative abundance of AOA versus AOB from oxygenated to low oxygen conditions in Saanich Inlet will help to resolve this.

5. Conclusions

Saanich Inlet is characterized by temporal and vertical oxygen gradients that modulate nitrogen speciation, N_2O distribution, and production pathways. The oxic-anoxic interface marks the boundary between net N_2O production and consumption zones, which were indicated by N_2O supersaturation and undersaturation, respectively. Above the interface, both ^{15}N tracer incubation experiments and in situ SP values confirmed that NH_4^+ oxidation is the dominant N_2O production pathway, probably causing N_2O supersaturation and contributing to N_2O efflux to the atmosphere. We conclude that elevated N_2O production from NH_4^+ oxidation following the autumn renewal event contributed to the increase of water column ΔN_2O from August to October. Pronounced N_2O undersaturation within the anoxic zone indicates net N_2O consumption in the near absence of NO_3^- and NO_2^-. Such a highly reducing environment could be a net N_2O sink when oxygen, NO_3^-, and NO_2^- are depleted, for example, removing N_2O transported into the anoxic zone from the oxycline through advection/diffusion. As shown by incubation experiments, addition of NO_3^- and NO_2^- to anoxic samples stimulated N_2O production. Conversely, reoxygenation of anoxic samples stimulated N_2O production from NH_4^+ oxidation. In comparison to open ocean OMZs, Saanich Inlet has high NH_4^+ fluxes (0.6–3.5 nmol m^{-2} s^{-1}) from the anoxic depths that can support nitrification and associated N_2O production. The dominance of NH_4^+ oxidation in N_2O production in Saanich Inlet is a combination of three factors: (1) water column suboxic conditions, (2) relatively high nitrification rates (few hundred nanomole per liter per day) supported by high NH_4^+ fluxes from the anoxic layer, and (3) depletion of NO_2^- and NO_3^- inhibiting partial denitrification to produce N_2O in suboxic and anoxic depths.

Data Availability Statement

Readers may find all the published data in PANGAEA Repository (https://doi.pangaea.de/10.1594/PANGAEA.912191).

Acknowledgments
The authors thank Roberta Hamme and Erinn Raftery (UVic) for their generous assistance in oxygen measurements. During field sampling, Catherine Stevens and Sarah Thornton (UVic), Shirley Lyons (Victoria Capital Regional District), and Lu Guan (Ocean Networks Canada) provided valuable technical guidance. Laboratory analyses of oxygen concentrations in sample vials at the end of incubation experiments were completed with help from Amy Maas (BIOS). We thank Captain Ken Brown and crew members of the *R/V Strickland* for their professional seamanship. Financial support for this study was provided by a grant from the cluster of excellence "The Future Ocean" to D. Grundle and C. Marandino (GEOMAR), the German Research Foundation Collaborative Research Centre 754 (www.sfb754.de), and a German Research Foundation grant to D. Grundle and C. Marandino (GR4731/2-1 and MA6297/3-1). B. Jameson was supported by the Canadian Healthy Oceans Network, University of Victoria, and NSERC CGS-M. Q. Ji was additionally supported by the Grant-In-Aid program at the Bermuda Institute of Ocean Sciences.

References

Anderson, J. J., & Devol, A. H. (1973). Deep water renewal in Saanich Inlet, an intermittently anoxic basin. *Estuarine and Coastal Marine Science*, *1*(1), 1–10. https://doi.org/10.1016/0302-3524(73)90052-2

Bange, H. W., Arévalo-Martínez, D. L., La Paz, M. D., Farias, L., Kaiser, J., Kock, A., et al. (2019). A harmonized nitrous oxide (N_2O) ocean observation network for the 21st century. *Frontiers in Marine Science*, *6*. https://doi.org/10.3389/fmars.2019.00157

Bange, H. W., Rapsomanikis, S., & Andreae, M. O. (1996). Nitrous oxide in coastal waters. *Global Biogeochemical Cycles*, *10*(1), 197–207. https://doi.org/10.1029/95GB03834

Bourbonnais, A., Lehmann, M. F., Hamme, R. C., Manning, C. C., & Juniper, S. K. (2013). Nitrate elimination and regeneration as evidenced by dissolved inorganic nitrogen isotopes in Saanich Inlet, a seasonally anoxic fjord. *Marine Chemistry*, *157*, 194–207. https://doi.org/10.1016/j.marchem.2013.09.006

Bristow, L. A., Dalsgaard, T., Tiano, L., Mills, D. B., Bertagnolli, A. D., Wright, J. J., et al. (2016). Ammonium and nitrite oxidation at nanomolar oxygen concentrations in oxygen minimum zone waters. *Proceedings of the National Academy of Sciences*, *113*(38), 10601–10606. https://doi.org/10.1073/pnas.1600359113

Buitenhuis, E. T., Suntharalingam, P., & Le Quéré, C. (2018). Constraints on global oceanic emissions of N_2O from observations and models. *Biogeosciences*, *15*(7), 2161–2175. https://doi.org/10.5194/bg-15-2161-2018

Capelle, D. W., Hallam, S. J., & Tortell, P. D. (2019). Time-series CH_4 measurements from Saanich Inlet, BC, a seasonally anoxic fjord. *Marine Chemistry*, *215*, 103,664. https://doi.org/10.1016/j.marchem.2019.103664

Capelle, D. W., Hawley, A. K., Hallam, S. J., & Tortell, P. D. (2018). A multi-year time-series of N_2O dynamics in a seasonally anoxic fjord: Saanich Inlet, British Columbia. *Limnology and Oceanography*, *63*(2), 524–539. https://doi.org/10.1002/lno.10645

Carpenter, J. H. (1965). The Chesapeake Bay institute technique for the Winkler dissolved oxygen method. *Limnology and Oceanography*, *10*(1), 141–143. https://doi.org/10.4319/lo.1965.10.1.0141

Ciais, P., Sabine, C., Bala, G., Bopp, L., Brovkin, V., Canadell, J., et al. (2013). *Carbon and other biogeochemical cycles* (pp. 465–570). Cambridge, UK, and New York, NY.

Codispoti, L. A. (2010). Interesting times for marine N_2O. *Science*, *327*(5971), 1339–1340. https://doi.org/10.1126/science.1184945

Cohen, Y. (1978). Consumption of dissolved nitrous oxide in an anoxic basin, Saanich Inlet, British Columbia. *Nature*, *272*(5650), 235–237. https://doi.org/10.1038/272235a0

Coplen, T. B. (2011). Guidelines and recommended terms for expression of stable-isotope-ratio and gas-ratio measurement results. *Rapid Communications in Mass Spectrometry*, *25*(17), 2538–2560. https://doi.org/10.1002/rcm.5129

Crutzen, P. J. (1970). The influence of nitrogen oxides on the atmospheric ozone content. *Quarterly Journal of the Royal Meteorological Society*, *96*(408), 320–325. https://doi.org/10.1002/qj.49709640815

de Bie, M. J. M., Middelburg, J. J., Starink, M., & Laanbroek, H. J. (2002). Factors controlling nitrous oxide at the microbial community and estuarine scale. *Marine Ecology Progress Series*, *240*, 1–9. https://doi.org/10.3354/meps240001

Fuchsman, C. A., Murray, J. W., & Konovalov, S. K. (2008). Concentration and natural stable isotope profiles of nitrogen species in the Black Sea. *Marine Chemistry*, *111*(1), 90–105. https://doi.org/10.1016/j.marchem.2008.04.009

Fujii, A., Toyoda, S., Yoshida, O., Watanabe, S., Sasaki, K. i., & Yoshida, N. (2013). Distribution of nitrous oxide dissolved in water masses in the eastern subtropical North Pacific and its origin inferred from isotopomer analysis. *Journal of Oceanography*, *69*(2), 147–157. https://doi.org/10.1007/s10872-012-0162-4

Garcia, H. E., & Gordon, L. I. (1992). Oxygen solubility in seawater: Better fitting equations. *Limnology and Oceanography*, *6*(37), 1307–1312. https://doi.org/10.4319/lo.1992.37.6.1307

Gargett, A. E., Stucchi, D., & Whitney, F. (2003). Physical processes associated with high primary production in Saanich Inlet, British Columbia. *Estuarine, Coastal and Shelf Science*, *56*(5), 1141–1156. https://doi.org/10.1016/S0272-7714(02)00319-0

Grundle, D. S., & Juniper, S. K. (2011). Nitrification from the lower euphotic zone to the sub-oxic waters of a highly productive British Columbia fjord. *Marine Chemistry*, *126*(1), 173–181. https://doi.org/10.1016/j.marchem.2011.06.001

Grundle, D. S., Maranger, R., & Juniper, S. K. (2012). Upper water column nitrous oxide distributions in the northeast subarctic Pacific Ocean. *Atmosphere-Ocean*, *50*(4), 475–486. https://doi.org/10.1080/07055900.2012.727779

Grundle, D. S., Timothy, D. A., & Varela, D. E. (2009). Variations of phytoplankton productivity and biomass over an annual cycle in Saanich Inlet, a British Columbia fjord. *Continental Shelf Research*, *29*(19), 2257–2269. https://doi.org/10.1016/j.csr.2009.08.013

Hansen, H. P., & Koroleff, F. (1999). *Determination of Nutrients*. Weinheim, Germany: Wiley-VCH Verlag GmbH.

Herlinveaux, R. H. (1962). Oceanography of Saanich Inlet in Vancouver Island, British Columbia. *Journal of the Fisheries Research Board of Canada*, *19*(1), 1–37. https://doi.org/10.1139/f62-001

Holmes, R. M., Aminot, A., Kerouel, R., Hooker, B. A., & Peterson, B. J. (1999). A simple and precise method for measuring ammonium in marine and freshwater ecosystems. *Canadian Journal of Fisheries and Aquatic Sciences*, *56*, 1801–1808. https://doi.org/10.1139/f99-128

Horak, R. E. A., Qin, W., Bertagnolli, A. D., Nelson, A., Heal, K. R., Han, H., et al. (2018). Relative impacts of light, temperature, and reactive oxygen on thaumarchaeal ammonia oxidation in the North Pacific Ocean. *Limnology and Oceanography*, *63*(2), 741–757. https://doi.org/10.1002/lno.10665

Ji, Q., Altabet, M. A., Bange, H. W., Graco, M. I., Ma, X., Arévalo-Martínez, D. L., & Grundle, D. S. (2019). Investigating the effect of El Niño on nitrous oxide distribution in the eastern tropical South Pacific. *Biogeosciences*, *16*(9), 2079–2093. https://doi.org/10.5194/bg-16-2079-2019

Ji, Q., Buitenhuis, E., Suntharalingam, P., Sarmiento, J. L., & Ward, B. B. (2018). Global nitrous oxide production determined by oxygen sensitivity of nitrification and denitrification. *Global Biogeochemical Cycles*, *32*, 1790–1802. https://doi.org/10.1029/2018GB005887

Ji, Q., & Grundle, D. S. (2019). An automated, laser-based measurement system for nitrous oxide isotope and isotopomer ratios at nanomolar levels. *Rapid Communications in Mass Spectrometry*, *33*(20), 1553–1564. https://doi.org/10.1002/rcm.8502

Ji, Q., & Ward, B. B. (2017). Nitrous oxide production in surface waters of the mid-latitude North Atlantic Ocean. *Journal of Geophysical Research: Oceans*, *122*(3), 2612–2621. https://doi.org/10.1002/2016jc012467

Laperriere, S. M., Nidzieko, N. J., Fox, R. J., Fisher, A. W., & Santoro, A. E. (2019). Observations of variable ammonia oxidation and nitrous oxide flux in a eutrophic estuary. *Estuaries and Coasts*, *42*(1), 33–44. https://doi.org/10.1007/s12237-018-0441-4

Löscher, C. R., Kock, A., Könneke, M., LaRoche, J., Bange, H. W., & Schmitz, R. A. (2012). Production of oceanic nitrous oxide by ammonia-oxidizing archaea. *Biogeosciences*, *9*(7), 2419–2429. https://doi.org/10.5194/bg-9-2419-2012

Louca, S., Hawley, A. K., Katsev, S., Torres-Beltran, M., Bhatia, M. P., Kheirandish, S., et al. (2016). Integrating biogeochemistry with multiomic sequence information in a model oxygen minimum zone. *Proceedings of the National Academy of Sciences*, *113*(40), E5925–E5933. https://doi.org/10.1073/pnas.1602897113

Maavara, T., Lauerwald, R., Laruelle, G. G., Akbarzadeh, Z., Bouskill, N. J., Van Cappellen, P., & Regnier, P. (2019). Nitrous oxide emissions from inland waters: Are IPCC estimates too high? *Global Change Biology*, *25*(2), 473–488. https://doi.org/10.1111/gcb.14504

Manning, C. C., Hamme, R. C., & Bourbonnais, A. (2010). Impact of deep-water renewal events on fixed nitrogen loss from seasonally-anoxic Saanich Inlet. *Marine Chemistry*, *122*(1), 1–10. https://doi.org/10.1016/j.marchem.2010.08.002

Rees, A. P., Brown, I. J., Clark, D. R., & Torres, R. (2011). The Lagrangian progression of nitrous oxide within filaments formed in the Mauritanian upwelling. *Geophysical Research Letters*, *38*, L21606. https://doi.org/10.1029/2011GL049322

Santoro, A. E., Buchwald, C., McIlvin, M. R., & Casciotti, K. L. (2011). Isotopic signature of N_2O produced by marine ammonia-oxidizing archaea. *Science*, *333*(6047), 1282–1285. https://doi.org/10.1126/science.1208239

Santoro, A. E., Francis, C. A., De Sieyes, N. R., & Boehm, A. B. (2008). Shifts in the relative abundance of ammonia-oxidizing bacteria and archaea across physicochemical gradients in a subterranean estuary. *Environmental Microbiology*, *10*(4), 1068–1079. https://doi.org/10.1111/j.1462-2920.2007.01547.x

Timothy, D. A., & Soon, M. Y. S. (2001). Primary production and deep-water oxygen content of two British Columbian fjords. *Marine Chemistry*, *73*(1), 37–51. https://doi.org/10.1016/S0304-4203(00)00071-2

Torres-Beltrán, M., Hawley, A., Capelle, D., Bhatia, M., Durno, E., Tortell, P., & Hallam, S. J. (2016). Methanotrophic community dynamics in a seasonally anoxic fjord: Saanich Inlet, British Columbia. *Frontiers in Marine Science*, *3*, 268. https://doi.org/10.3389/fmars.2016.00268

Torres-Beltrán, M., Hawley, A. K., Capelle, D., Zaikova, E., Walsh, D. A., Mueller, A., et al. (2017). A compendium of geochemical information from the Saanich Inlet water column. *Scientific Data*, *4*(1), 1–11. https://doi.org/10.1038/sdata.2017.159

Toyoda, S., Yoshida, N., & Koba, K. (2017). Isotopocule analysis of biologically produced nitrous oxide in various environments. *Mass Spectrometry Reviews*, *36*(2), 135–160. https://doi.org/10.1002/mas.21459

Ward, B. B., & Kilpatrick, K. A. (1990). Relationship between substrate concentration and oxidation of ammonium and methane in a stratified water column. *Continental Shelf Research*, *10*(12), 1193–1208. https://doi.org/10.1016/0278-4343(90)90016-F

Weigand, M. A., Foriel, J., Barnett, B., Oleynik, S., & Sigman, D. M. (2016). Updates to instrumentation and protocols for isotopic analysis of nitrate by the denitrifier method. *Rapid Communications in Mass Spectrometry*, *30*(12), 1365–1383. https://doi.org/10.1002/rcm.7570

Weiss, R. F., & Price, B. A. (1980). Nitrous oxide solubility in water and seawater. *Marine Chemistry*, *8*(4), 347–359. https://doi.org/10.1016/0304-4203(80)90024-9

Westley, M. B., Yamagishi, H., Popp, B. N., & Yoshida, N. (2006). Nitrous oxide cycling in the Black Sea inferred from stable isotope and isotopomer distributions. *Deep Sea Research Part II: Topical Studies in Oceanography*, *53*(17), 1802–1816. https://doi.org/10.1016/j.dsr2.2006.03.012

Wilson, S. T., Bange, H. W., Arévalo-Martínez, D. L., Barnes, J., Borges, A. V., Brown, I., et al. (2018). An intercomparison of oceanic methane and nitrous oxide measurements. *Biogeosciences*, *15*(19), 5891–5907. https://doi.org/10.5194/bg-15-5891-2018

Yung, Y. L., Wang, W. C., & Lacis, A. A. (1976). Greenhouse effect due to atmospheric nitrous oxide. *Geophysical Research Letters*, *3*(10), 619–621. https://doi.org/10.1029/GL003i010p00619

Zaikova, E., Walsh, D. A., Stilwell, C. P., Mohn, W. W., Tortell, P. D., & Hallam, S. J. (2010). Microbial community dynamics in a seasonally anoxic fjord: Saanich Inlet, British Columbia. *Environmental Microbiology*, *12*(1), 172–191. https://doi.org/10.1111/j.1462-2920.2009.02058.x

Zakem, E. J., & Follows, M. J. (2017). A theoretical basis for a nanomolar critical oxygen concentration. *Limnology and Oceanography*, *62*(2), 795–805. https://doi.org/10.1002/lno.10461